

Michelson Interferometer

PY4113 Lab Report

University College Cork
School of Physics

Author: Jordan Darran Emmett Walsh (120387836)

Lab Partner: Rory Tomas Fox (120445052)

Location: Kane Building 202, University College Cork

Date: 15/11/23

Contents

| | |
|---|-----------|
| Introduction | 2 |
| 1.1 Motivation | 2 |
| 1.2 Fundamentals | 2 |
| Experimental Methods | 4 |
| 2.1 Calibration using HeNe laser | 5 |
| 2.2 Determination of emission wavelength of unknown laser diode | 6 |
| 2.3 Determination of the refractive index of air | 6 |
| Results | 7 |
| 3.1 Calibration | 7 |
| 3.2 Emission wavelength of unknown laser diode | 9 |
| 3.3 Refractive index of air | 9 |
| Discussion | 10 |
| Conclusion | 12 |
| A | 14 |
| A.1 Derivation of $S_0(\sigma)$ | 14 |
| B | 15 |
| B.1 Calibration Raw Data | 15 |
| B.2 Unknown Diode utilised measurement | 16 |
| B.3 Refractive Index Measurement Relevant Data | 16 |
| B.4 Other Measurements | 19 |

Michelson Interferometer

Introduction

This report details one of five experiments completed as part of enrollment in PY4113, the objective of which is to calibrate a Michelson interferometer setup using a known source (HeNe laser) and utilise it to determine the refractive index of air and emission wavelength of an unknown laser diode.

The report begins with a brief motivation and a discussion of fundamental concepts relevant to the Michelson Interferometer, including Fourier transform spectroscopy. The remainder of the report is structured typically, with sections for methodology, results (including error analysis where appropriate), discussion, and conclusion.

1.1 Motivation

An interferometer is a device that uses variations in the phase of a signal as it travels along distinct paths of adjustable length [1]. Optical Interferometers are used for wave-length and atmosphere refractive index measurements [2], gas flow measurements in wind tunnels [3] and recently they have been particularly important for Astrophysics and Astronomy [4]. An astronomical interferometer combines separate telescopes, mirror segments, or radio telescope antennas through interferometry to achieve higher-resolution imaging of celestial objects.

The Michelson-Morley experiment was first conducted in 1887 and sought to address the nature of the medium through which light waves propagate [6] [7]. Utilised was the Michelson interferometer, a precision measurement tool invented by Albert A. Michelson. At the time the notion was that if the Earth was in motion within a fixed dark energy field (the "luminiferous aether"^[7], which was theorised to be the one "true" inertial frame), such movement could be identified through a Lorentz violation [7]. The experiment failed to detect the aether, leading ultimately to the development of special relativity (A. Einstein 1905).

More recently, the observation of a gravitational-wave signal produced by the coalescence of two stellar-mass black holes ("gravitational-wave strain"^[5]) was detected with the use of modified Michelson Interferometers with arms over 4km in length [5].

1.2 Fundamentals

Interferometer Operation

An interferometer is a device that uses variations in the phase of a signal as it travels along distinct paths of adjustable length [1]. A schematic representation of a Michelson interferometer is shown in Fig 1.1. An incident plane wave from the source is separated into two waves of equal magnitude.

The reflected and transmitted beams travel along two different optical paths r_1 and r_2 where they independently pick up a phase due to differences in path length or propagation material. If coupled correctly, both waves are reflected by mirrors back along the same path to the beam splitter where recombination occurs and interference can be observed at the plane of the detector. The interferometer generates two separate output waves, unlike that of something like a Mach-Zhender structure.

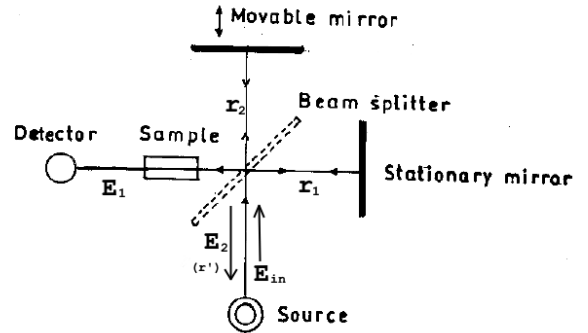


Figure 1.1: [8] Ray diagram for Michelson interferometer.

Mathematically, with reference to Fig 1.1, the system can be described as

$$\begin{aligned} E_{in} &= E_0 e^{-i(\omega t - kr)} \\ E_1 &= \frac{1}{2} E_{in}(r, t) (e^{-ikr_1} + e^{-ikr_2}) \\ E_2 &= \frac{1}{2} E_1 e^{-i(\omega t - kr')} (e^{-ikr_1} - e^{-ikr_2}) \end{aligned}$$

as per [9] verbatim. We are interested only in output E_1 , which has an intensity of

$$\begin{aligned} I &= \frac{1}{2} \epsilon_0 c E * E^* \\ I_1 &= \frac{1}{2} I_0 (1 + \cos[2k(r_1 - r_2)]) \\ &\equiv \frac{1}{2} I_0 (1 + \cos[2\pi\sigma\Delta r]) \end{aligned}$$

where $\sigma = \frac{1}{\lambda}$. This shows us that the difference in path length ($r_1 - r_2$) impacts the observed intensity sinusoidally, and that due to the splitting of the output one does not observe total destructive interference.

Fourier Transform Spectroscopy

By motorizing the movable mirror in Fig 1.1, time-dependant interference at the detector enables measurement of the temporal coherence of light at various time delays, effectively transforming the time domain into a spatial coordinate. One can reconstruct the frequency spectrum of the input by taking intensity measurements at multiple discrete positions of the movable mirror and applying a Fourier transform to the resulting temporal coherence of the light.

The waveform obtained is therefore a discrete representation of the continuous signal,

$$x[n] = A \cos(2\pi f n + \phi)$$

where A is the amplitude of the signal, f is the frequency and ϕ is the phase with N total samples [9]. It's corresponding discrete Fourier transform is

$$X[k] = \sum_{n=0}^{N-1} x[n] e^{-j2\pi k \frac{n}{N}}$$

The interferogram $I(x)$ produced by the setup discussed can be expressed by the product of a cosine multiplied by the boxcar function $\beta(x)$

$$I(x) = A \cos(x) \beta(x)$$

This equivalence is used in the explicit calculation of the Fourier transform of the interferogram [9], where

$$\begin{aligned} S_0(\sigma) &= \int_{-\infty}^{\infty} I(\Delta r) e^{i2\pi\sigma\Delta r} d\Delta r \equiv A \mathcal{F}\{\cos(\Delta r)\} * \mathcal{F}\{\beta(\Delta r)\} \\ \implies S_0(\sigma) &= \pi \Delta r_0 \{ \text{sinc}[2\pi(\sigma - \sigma_0)\Delta r_0] + \text{sinc}[2\pi(\sigma + \sigma_0)\Delta r_0] \} \end{aligned} \quad (1.1)$$

which has been fully derived in A.1. $\delta\sigma = \frac{1}{\Delta r_0}$ is therefore a measure of the spectrometers ability to distinguish adjacent spectral lines [9] with Δr_0 "the length of the optical path used in the interferometric measurement" [9].

Experimental Methods

This section details the methods and apparatus utilised. Methods to demonstrate the discussed principles of Fourier Transform spectroscopy, determine emission wavelength of a device, and determine the refractive index of a sample are discussed.

Apparatus

HeNe laser (JDS Uniphase) with a 632.8nm emission wavelength for interferometer calibration, unknown red laser diode, Michelson interferometer setup with an 18mm convex lens, 48mm convex lens, a Thorlabs PDA36A-EC Si detector, DC servo actuator-driven motorized translation stage, and vacuum chamber with hand operated pump.

Laser Safety

The minimum safe operating distance of the diode laser can be calculated using the 'Nominal Ocular Hazard Distance' (NOHD) formula [10]:

$$NOHD = 2 \sqrt{\frac{P}{MPE\pi\theta_1\theta_2}}$$

where MPE is Maximum Permissible Exposure, θ is beam divergence and P is optical power. For general lab use we will assume a blink-reflex accidental exposure time of 0.25s. According to [11], the MPE of a 632nm laser is

$$\begin{aligned} MPE &= 18t^{0.75} Jm^{-2} \\ &= 18(0.25)^{0.75} Jm^{-2} \\ &= 6.3639 Jm^{-2} \\ &\equiv 25.45 Wm^{-2} \end{aligned}$$

According to the JDS Uniphase HeNe Laser specification sheet [12], the minimum perpendicular and parallel divergence angles of the laser are

$$\begin{aligned}\theta_{\parallel} &= \theta_1 = 1.7\text{mrad} \\ \theta_{\perp} &= \theta_2 = 1.7\text{mrad}\end{aligned}$$

We consider the minimum divergences as to maximise the potential optical power density. $P \approx 1\text{mW}$ is the power the laser is capable of [12]. Therefore, we can conclude

$$NOHD = 2\sqrt{\frac{1\text{mW}}{25.45[\text{Wm}^{-2}]\pi(1.7\text{mrad})^2}} = 4.16\text{m}$$

This laser is dangerous, as noted by the warning sticker on the top of it. It was ensured that the laser at no point was directed at another person. Since the laser was used in conjunction with a convex lens, it posed significantly less threat (due to further beam divergence) than outlined.

2.1 Calibration using HeNe laser

The DC servo actuator-driven motorized translation stage, with a 20 nm resolution, is employed for continuous mirror displacement. Direct translation with the stage at 1/30 of the laser wavelength resolution is insufficient for precise interferometric measurements, necessitating an internal mechanism for fine mirror M2 displacement. The calibration in question is of an unknown conversion factor of relative motor displacement to actual motor displacement which arises from the mechanism used to displace the moving mirror.

Setup/Procedure

The experiment was setup as shown in Fig 1.1, with the HeNe laser in place as the source and coupled such that interference rings were visible on the plane of the detector (this was done using a non-reflective piece of card at the detector and careful positioning of optics). The detector in Fig 1.1 was the Thorlabs PDA36A-EC Si detector. The procedure was followed verbatim to [9]; A LabView program '*interferometer operation.vi*' was utilised to control the motorized mirror and recorded the intensity incident on the Si detector as a function of mirror displacement. This was done for various program parameters '*move relative distance*' [mm] and '*data displacement step*' with '*set speed*' = 0.01 [mm/s] unchanged throughout all measurements.

Analysis

Analysis was done using another LabVIEW VI, '*fourier transform of data.vi*', which requires the aforementioned conversion factor to operate. Since we know the emission wavelength of the HeNe laser is 632.8nm [9] [12], the conversion factor was tuned until the peak of the obtained Fourier Transform/Optical spectrum peaked at 632.8nm.

2.2 Determination of emission wavelength of unknown laser diode

Setup/Procedure

The experiment was setup as shown in Fig 1.1, with the unknown laser diode in place as the source and coupled such that interference rings were visible on the plane of the detector (this was again done using a non-reflective piece of card at the detector and careful positioning of optics). The procedure was followed verbatim to [9]; A LabView program '*interferometer operation.vi*' was utilised to control the motorized mirror and recorded the intensity incident on the Si detector as a function of mirror displacement.

Analysis

Using the previously determined conversion factor for '*fourier transform of data.vi*' and importing relevant data obtained by the procedure above, the emission wavelength of the unknown laser diode could be determined by observing the program output and locating the corresponding peak wavelength in the FFT.

2.3 Determination of the refractive index of air

Setup/Procedure

The experiment was setup as shown in Fig 1.1, with the HeNe laser diode in place as the source and coupled such that interference rings were visible on the plane of the detector (this was again done using a non-reflective piece of card at the detector and careful positioning of optics). An evacuated chamber with hand operated pump was placed in the position of 'sample' shown in Fig 1.1.

The procedure was followed verbatim to [9]; Air was removed from the chamber until a significant vacuum was achieved. A LabView program '*refractive index measurement.vi*' was utilised to recorded the variation of incident intensity on the Si detector as a function of time. As the code was started, air was reintroduced into the chamber by gently releasing the red valve at the bottom of the gauge. Data acquisition was stopped once the chamber was fully relieved. The data was saved, and the process was repeated a further 4 times.

Analysis

This setup causes an optical path length change in one arm of

$$\Delta\phi = 4\pi\Delta n\sigma\Delta r_c$$

where Δr_c is the length of the chamber, $\sigma = \frac{1}{\lambda}$ is the wavenumber and Δn is the change in refractive index from the chamber's vacuum state to it's aerated state [9]. The number of fringes/peaks in the signal observed (LabView data) can be interpreted as an integer m number of 2π phase shifts such that $\Delta\phi = 2\pi m$. Knowing that $n_{vac} = 1$, it suffices to show that

$$\Delta n = \frac{\lambda m}{2\Delta r_c} \quad (2.2)$$

$$n_{air} = 1 + \Delta n \quad (2.3)$$

Results

The following sub-sections compile and analyse the relevant data obtained by the procedures and methods outlined above.

Please Note: corresponding units for 'light intensity' were not provided or referenced in program code or guidelines [9]; as such they have been labelled arbitrary (au).

3.1 Calibration

Fig 3.2 shows the resulting transformation obtained from the procedure outlined in section 2.1. To keep this report concise, where applicable only resulting transforms such as that in Fig 3.2 (b) will be shown in the main text. However, all relevant raw data and figures can be found in B.1 and will be referenced accordingly.

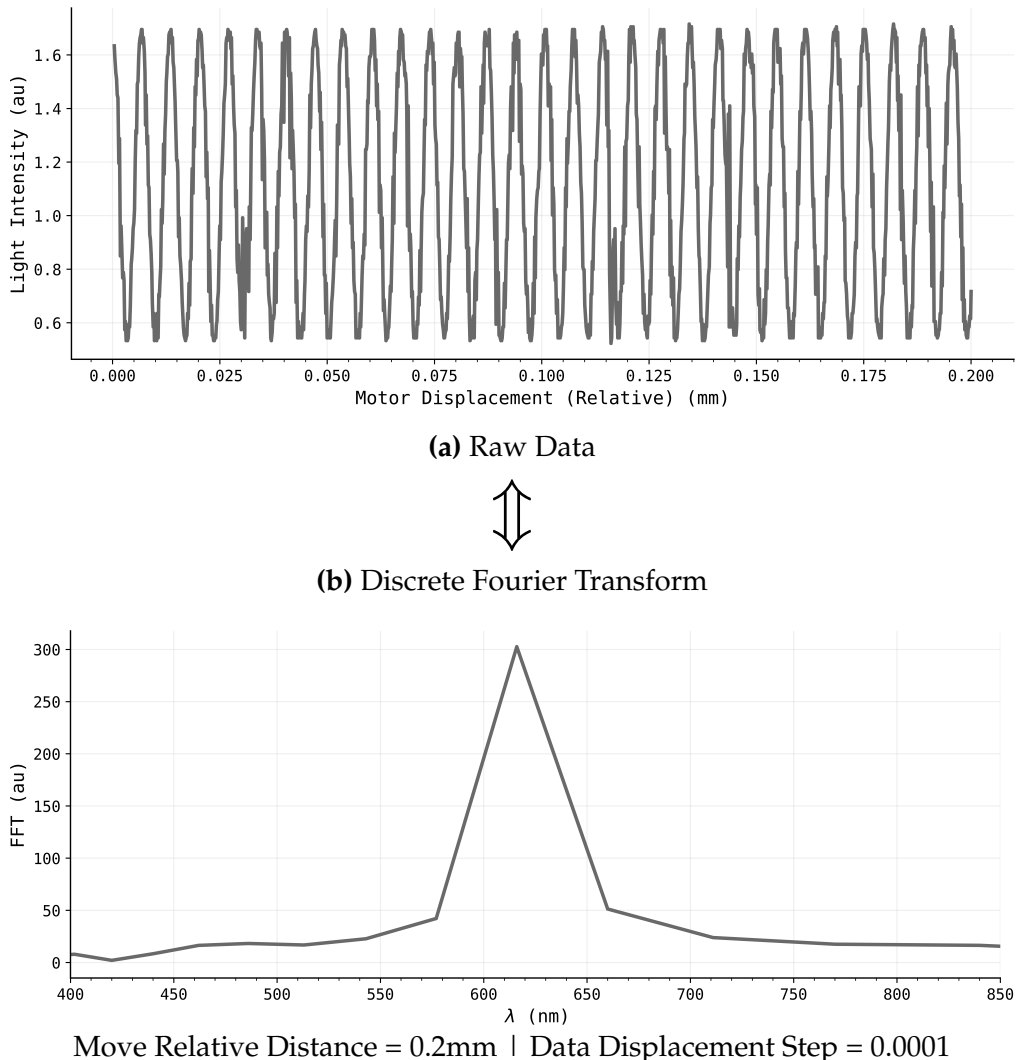
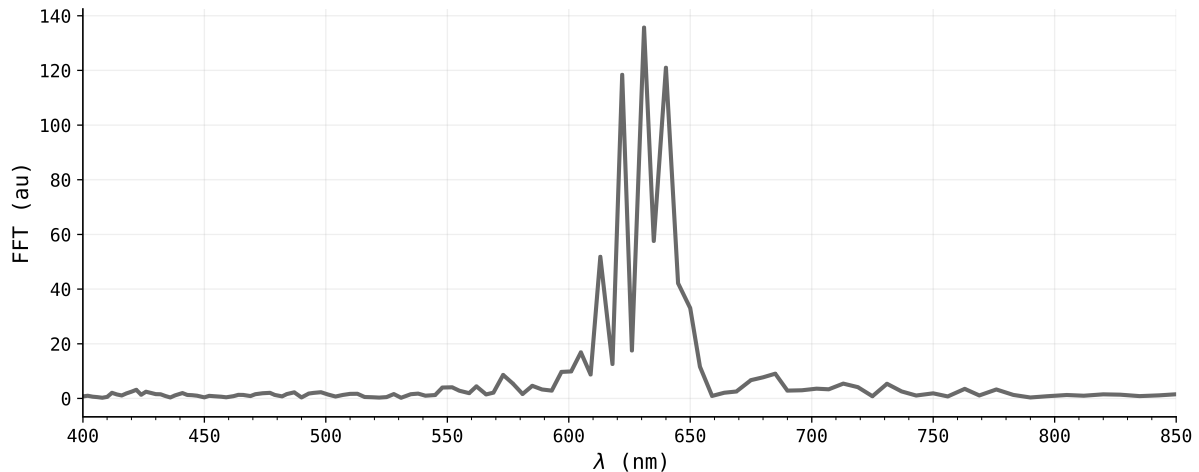
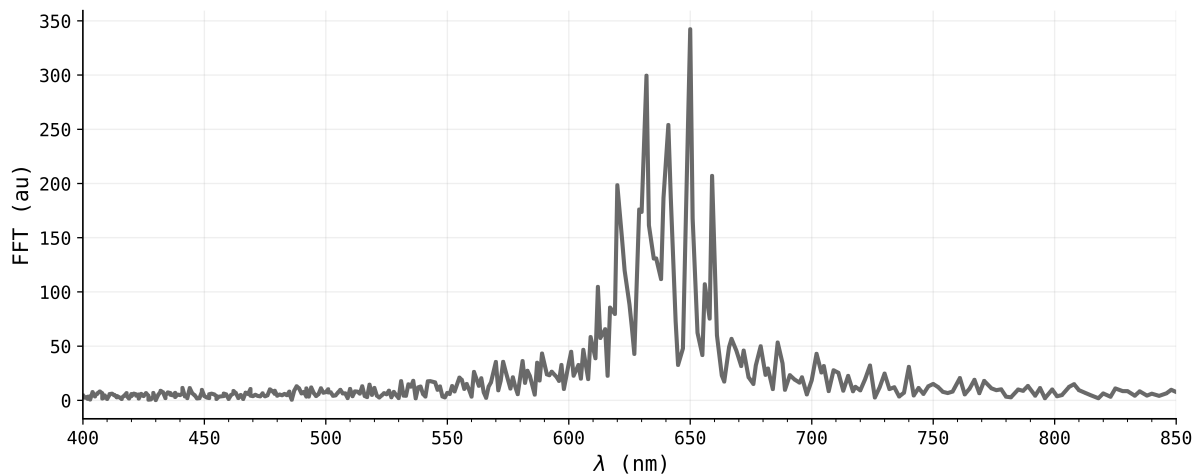


Figure 3.2: Intensity profile for relative motor displacement and resulting transformation/frequency spectrum obtained from the procedure outlined in section 2.1.



Move Relative Distance = 0.95mm | Data Displacement Step = 0.0002

Figure 3.3: Resulting transformation/frequency spectrum obtained from the procedure outlined in section 2.1. Corresponding raw data is shown in Fig B.1



Move Relative Distance = 2.95mm | Data Displacement Step = 0.0001

Figure 3.4: Resulting transformation/frequency spectrum obtained from the procedure outlined in section 2.1. The HeNe laser has strong spectral components about its central wavelength approximately every $\Delta\lambda = 9\text{nm}$. Corresponding raw data is shown in Fig B.2

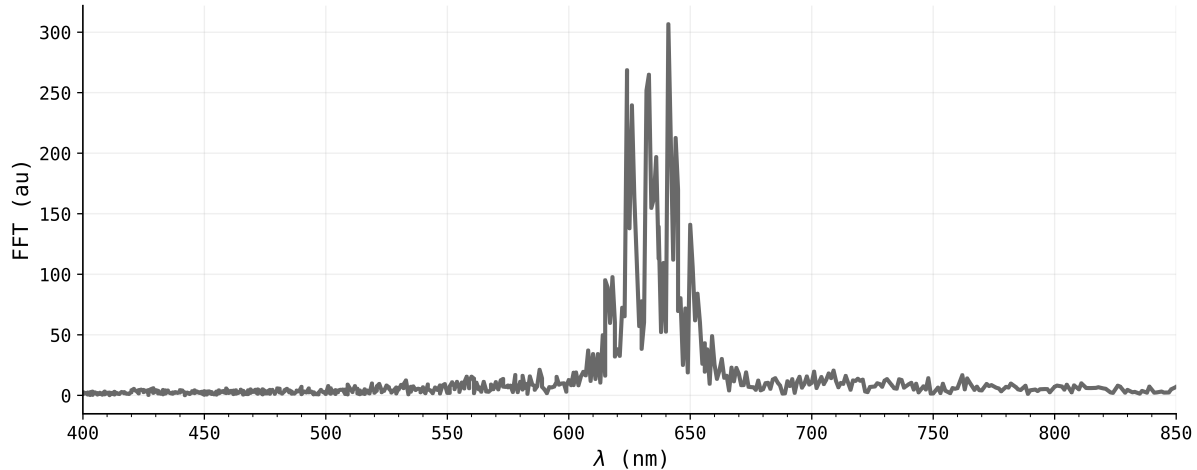
It is apparent from the results shown in Fig 3.2, 3.3, 3.4 that extending the physical travel distance of the mirror in the interferometer the spectral resolution is improved. Recording more data points over an extended path length results in a more detailed sampling of the signal. As a result, the Fourier transform can capture higher-frequency components with greater precision, enhancing the determined spectrum.

Conversion Factor

By the process outlined in section 2.1, the conversion factor η was determined to be

$$\overline{\eta} = 0.04165 \pm 0.00005$$

3.2 Emission wavelength of unknown laser diode



Move Relative Distance = 5.00mm | Data Displacement Step = 0.0001

Figure 3.5: Resulting transformation/frequency spectrum obtained from raw data as shown in Fig B.3. The central wavelength of the unknown laser diode is $\lambda = 632\text{nm}$ uncertainty in λ was determined qualitatively as the spectral resolution. The modal peaks are spaced approximately $\Delta\lambda = 8\text{nm}$ apart.

$$\boxed{\lambda_{unk} = (633 \pm 1)\text{nm}}$$

3.3 Refractive index of air

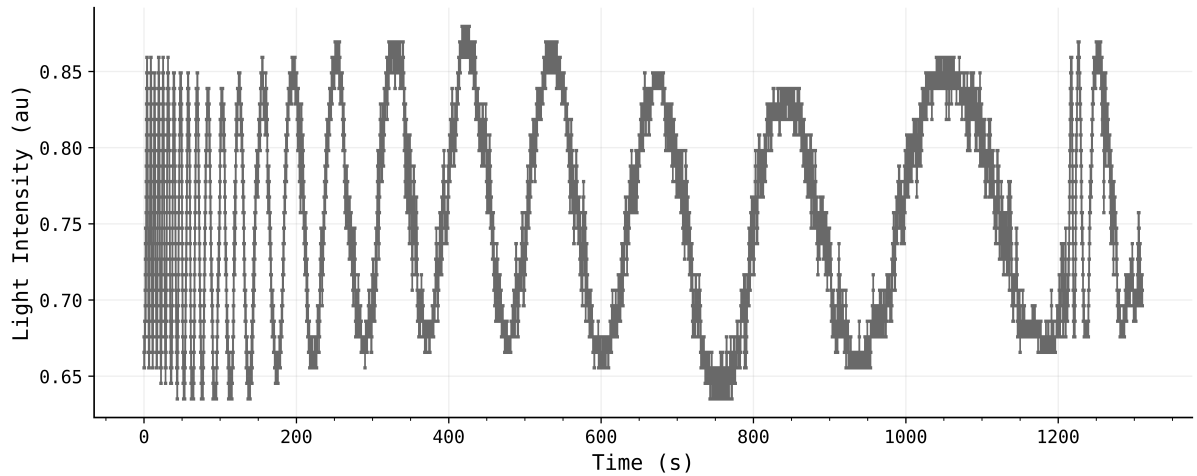


Figure 3.6: Example refractive index measurement. As the measurement began, air was reintroduced into the evacuated chamber by gently releasing the red valve at the bottom of the gauge. Data acquisition was stopped once the chamber was fully relieved. The number of fringes to be observed in this example is $m = 24$. All measurements can be found in B.4.

| λ (nm) | Δr_c (mm) |
|----------------|-------------------|
| 632.8 ± 4 | 37.8 ± 0.1 |

Table 3.1: Utilised parameters for calculation in Tab 3.2 and uncertainties for subsequent error analysis. Uncertainty in lambda was taken as 4.5nm, the reason for this is that we observed strong spectral components at $\Delta\lambda \approx 9\text{nm}$ in Fig 3.4, however we know the laser should be monochromatic so an intermediate to contradicting factors could be $\delta\lambda = 4.5\text{nm}$.

| Fig | m | Δn |
|-----|-----|-------------|
| 3.6 | 24 | 0.000200889 |
| B.5 | 23 | 0.000192519 |
| B.4 | 26 | 0.00021763 |
| B.6 | 27 | 0.000226 |
| B.7 | 26 | 0.00021763 |

$$\Delta n_{avg} = 0.000210933 \mid \sigma_{\Delta n} = 1.23 \times 10^{-5}$$

$$m_{avg} = 25.2 \mid \sigma_m = 1.4696$$

Table 3.2: Number of fringes determined air was reintroduced into the evacuated chamber by across 5 runs. m is the number of relevant fringes observed. Δn is the corresponding change in refractive index as the chamber is aerated. 'Fig' refers to the relevant figure from which m was determined. σ_x is the standard deviation in x . Relevant raw data can be found in B.4 as referenced.

Error Analysis

From the analysed data shown in Tab 3.2 and uncertainties in Tab 3.1 it suffices to show

$$\begin{aligned} \frac{\delta n}{\Delta n} &= \frac{\delta\lambda}{\lambda} + \frac{\delta r_c}{\Delta r_c} + \frac{\delta m}{m} \\ &= \frac{8}{632.8} + \frac{0.05}{37.8} + \frac{1.4696}{25.2} \\ &= 0.06728 \\ \implies \delta n &= 1.41 \times 10^{-5} \end{aligned}$$

This variation is on the same order of that determined by $\sigma_{\Delta n}$. The refractive index of air is shown to be

$$\underline{n_{air} = 1.00021 \pm 0.00001}$$

Discussion

The interferometer is believed to be correctly calibrated with a conversion factor $\eta = 0.04165 \pm 0.00005$. This conclusion was drawn as at this uncertainty the variation in the central peak was negligible or unobserved. An additional investigation was undertaken to further confirm this conversion. The '*interferometer operation.vi*' program

parameters were chosen seemingly at random, 3 very different cases were recorded and exported to '*fourier transform of data.vi*', where the conversion factor $\eta = 0.04165$ was used to transform the data. Fig 4.7 shows that this made no difference to the positioning of HeNe central peak, showing a disconnect between the conversion factor and sampling conditions of the program. Where this had previously been unclear (as discussed with lab demonstrator), it suffices to conclude that the conversion factor is directly related to motor displacement, and the validity of resulting transforms is not affected by conditions such as the 'set speed' or 'move relative distance'.

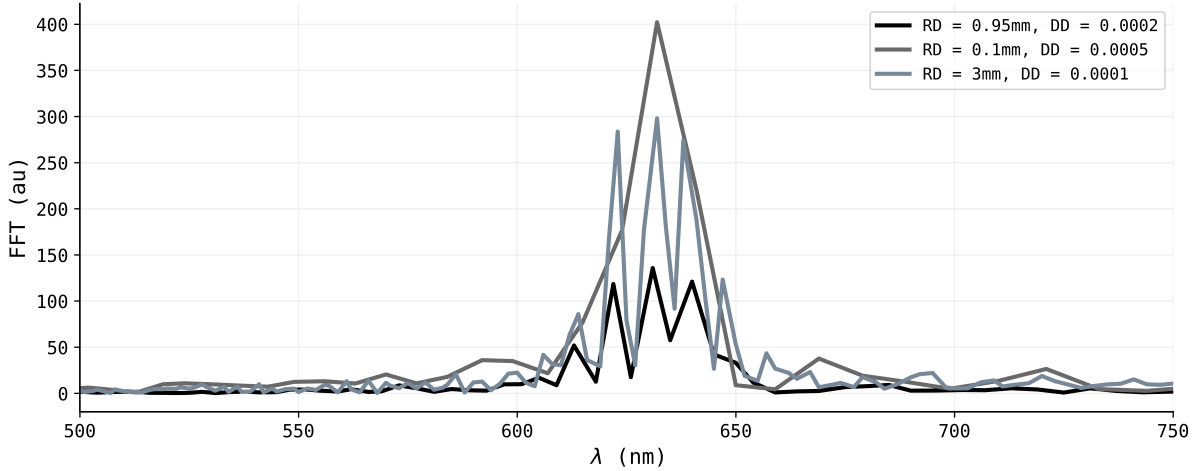


Figure 4.7: Various HeNe laser spectra verifying determined conversion factor. Resulting transformations obtained from raw data under various '*interferometer operation.vi*' program parameters. RD = 'Move Relative Distance', SS = 'Set Speed', DD = 'Data Displacement'. This concludes that the conversion factor is directly related to motor displacement, and the validity of resulting transforms is not affected by conditions such as the 'set speed' or 'move relative distance'. This had previously been unclear.

It is apparent from the results shown in Fig 3.2, 3.3, 3.4 that extending the physical travel distance of the mirror in the interferometer improves spectral resolution. Recording more data points over an extended path length results in a more detailed sampling of the signal. As a result, the Fourier transform can capture higher-frequency components with greater precision, enhancing the determined spectrum. The spectral resolution for this setup is defined as [9]

$$\delta\sigma = \frac{1}{\Delta r_0} \quad (4.4)$$

where Δr_0 is "*the length of the optical path used in the interferometric measurement*"^[9]. This definition could not be found from any other source. The corresponding spectral resolutions are tabulated in Tab 4.3 using Eq 4.4.

[9] states "*A Helium Neon laser, in optimal conditions, operates as single mode monochromatic light source. A red emitting laser diode is instead a multimode monochromatic light source with each mode separated by $\Delta\lambda = 0.1 \text{ nm}$. If the resolution is not sufficiently small, these modes are seen by the spectrometer as a single spectral line. Consequently, the spectra of the Helium Neon laser and of the laser diode are structurally identical.*"^[9] This has been quoted directly because, none of these features are observed as stated. The Helium Neon laser does not act as a single mode source, as demonstrated in Fig 3.2, 3.3,

| Fig | Δr_0 (mm) | $\delta\sigma$ (mm $^{-1}$) |
|-----|-------------------|------------------------------|
| 3.2 | 0.2 | 5 |
| B.8 | 0.5 | 2 |
| 3.3 | 0.95 | 1.05263 |
| 3.4 | 2.95 | 0.338983 |
| 3.5 | 5 | 0.2 |

Table 4.3: Spectral resolution for relevant measurements, as specified to be included in this report [9]. It is difficult to determine a physical interpretation of $\delta\sigma$ given it's units of [mm $^{-1}$], [9] states it to simply be a measure of precision. With that in mind, the conclusion here is that a smaller $\delta\sigma$ provides improved resolution and this is achieved by increasing path length Δr_0 .

3.4, it has modal components to its spectra separated at $\Delta\lambda \approx 9\text{nm}$, unless of course these do not exist and are an unintentional by-product of the custom implemented Fourier Transform algorithm. The unknown laser diode has spectral modes separated at $\Delta\lambda \approx 8\text{nm}$ apart, as shown in Fig 3.5. The only part of this statement that has actually been observed is that the spectra are structurally identical (but confusingly not for the reason stated). Consequently, by virtue of the quoted statement, one is led to conclude that the resolution is not "sufficiently small", as it is difficult to believe that the two lasers are exactly identical when their lasing mechanism and structure are totally foreign from each other. If the claims of [9] (lab guidelines) are true, then there is an issue with the current setup.

The refractive index of air was determined to be $n_{air} = 1.00021 \pm 0.00001$. This is a reasonably good calculation, given that it is on the same order of magnitude as the actual refractive index of air, which is documented to be $n_{air} = 1.00028$ [13]. While this does not lie within our margin of error, this can be drawn mostly to the fact that the hand operated pump did not create a convincingly strong enough vacuum to warrant the analytical treatment received (it was assumed that the transition in the chamber was from a prefect vacuum to atmospheric pressure). The pump gauge at its peak vacuum could not even reach the specified 700cm mercury vacuum in [9].

Two uncertainties had been determined for n_{air} , both of which were on the same order. The small experimental error determined can be eluded to the accuracy and precision of the Michelson interferometer, our figure is incorrect due to either the vacuum pump or possibly under counting of fringes. Perhaps there was more fringes to be observed in the measurements and data acquisition had been prematurely cut.

Conclusion

A Michelson interferometer setup is calibrated using a known HeNe laser. The setup is utilised to demonstrate principles of Fourier Transform spectroscopy and identify spectral features of the HeNe laser. Extending the physical travel distance of the mirror in the interferometer improves spectral resolution, as recording more data points over an extended path length results in a more detailed sampling of the signal. The setup is further utilised to determine the wavelength of an unknown laser diode. Ambiguities are identified in the determined spectra between the calibration laser and unknown. Notably, identical modal spacing ($\Delta\lambda = 8\text{nm}/9\text{nm}$) is observed, contradicting pro-

vided information about the lasers in use. The refractive index of air is determined to the same order of magnitude as that of literature using the Michelson interferometer and evacuated chamber with hand operated pump.

References

- [1] Three Centimeter Microwave Apparatus Operating Instructions, **Central Scientific Company**, Interferometer section and discussion.
- [2] H. Matsumoto, Y. Zhu, S. Iwasaki, T. O'ishi, "Measurement of the changes in air refractive index and distance by means of a two-color interferometer," Appl. Opt. 31, 4522-4526 (1992)
- [3] M. R. Fulghum "Turbulence measurements in high-speed wind tunnels using focusing laser differential interferometry," The Pennsylvania State University ProQuest Dissertations Publishing, 2014. 3690119.
- [4] O. von dcr Lühe, "An Introduction to Interferometry with the ESO Very Large Telescope", **European Southern Observatory**
- [5] B. P. Abbott et al. "GW151226: Observation of Gravitational Waves from a 22-Solar-Mass Binary Black Hole Coalescence, (LIGO Scientific Collaboration and Virgo Collaboration), PRL 116, 241103 (2016)
- [6] R. S. Shankland, "Michelson-Morley Experiment" Am. J. Phys. 1 January 1964; 32 (1): 16–35
- [7] A. A Michelson, E. W Morley, *On the Relative Motion of the Earth and the Luminiferous Ether*, American Journal of Science, Vol. 34, pp. 333–345, 1887.
- [8] Jaggi, Neena & Vij, D.R. (2007). FOURIER TRANSFORM INFRARED SPECTROSCOPY. 10.1007/0-387-37590-2_9.
- [9] PY4113 Michelson Interferometer Guidelines, University College Cork
- [10] University College Cork Laser Safety Guidelines and supplementary course notes (2022)
- [11] University College Cork Laser Safety Tables (v5), "Annexes to course on; Lasers and Laser Safety"
- [12] JDS UNIPHASE Model 1508-1 Helium Neon Gas Laser Novette T8015680 Specification Sheet
- [13] P. E. Ciddor. Refractive index of air: new equations for the visible and near infrared, Appl. Optics 35, 1566-1573 (1996) obtained via 'refractiveindex.info'

Appendix A

A.1 Derivation of $S_0(\sigma)$

Derivation as specified to be shown by [9].

$$I(x) = A \cos(x) \beta(x)$$

$$\begin{aligned} S_0(\sigma) &= \int_{-\infty}^{\infty} I(\Delta r) e^{i2\pi\sigma\Delta r} d\Delta r \\ &= \int_{-\infty}^{\infty} A \cos(\Delta r) \beta(\Delta r) e^{i2\pi\sigma\Delta r} d\Delta r \\ &\equiv A \mathcal{F}\{\cos(\Delta r)\} * \mathcal{F}\{\beta(\Delta r)\} \end{aligned}$$

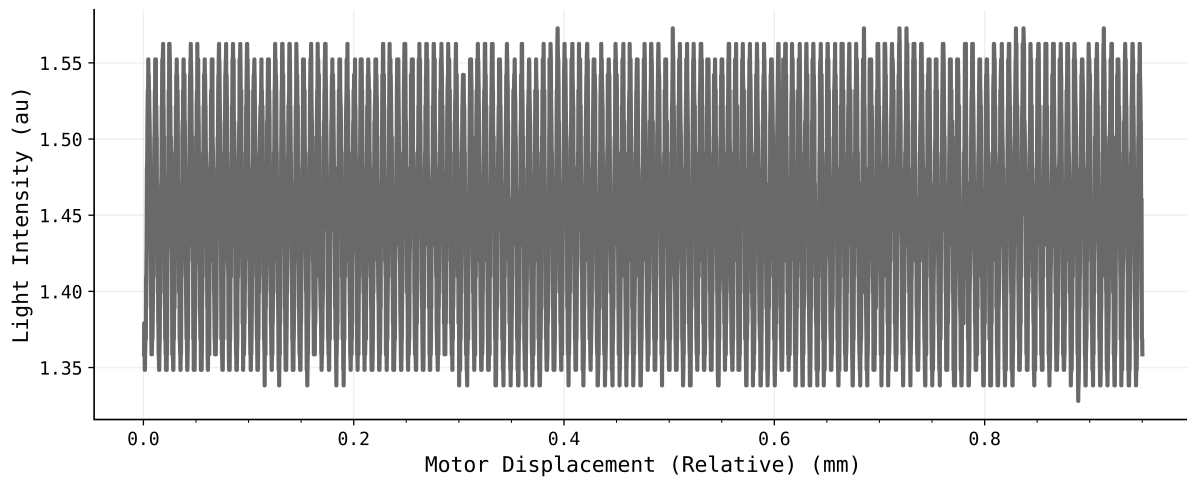
$$\mathcal{F}\{\cos(\Delta r)\} = \pi[\delta(2\pi\sigma - 2\pi\sigma_0) + \delta(2\pi\sigma + 2\pi\sigma_0)]$$

$$\mathcal{F}\{\beta(\Delta r)\} = \Delta r_0 \text{sinc}\left(\frac{2\pi\sigma\Delta r_0}{2\pi}\right) = \Delta r_0 \text{sinc}(\sigma\Delta r_0)$$

$$\implies S_0(\sigma) = \pi \Delta r_0 \{\text{sinc}[2\pi(\sigma - \sigma_0)\Delta r_0] + \text{sinc}[2\pi(\sigma + \sigma_0)\Delta r_0]\}$$

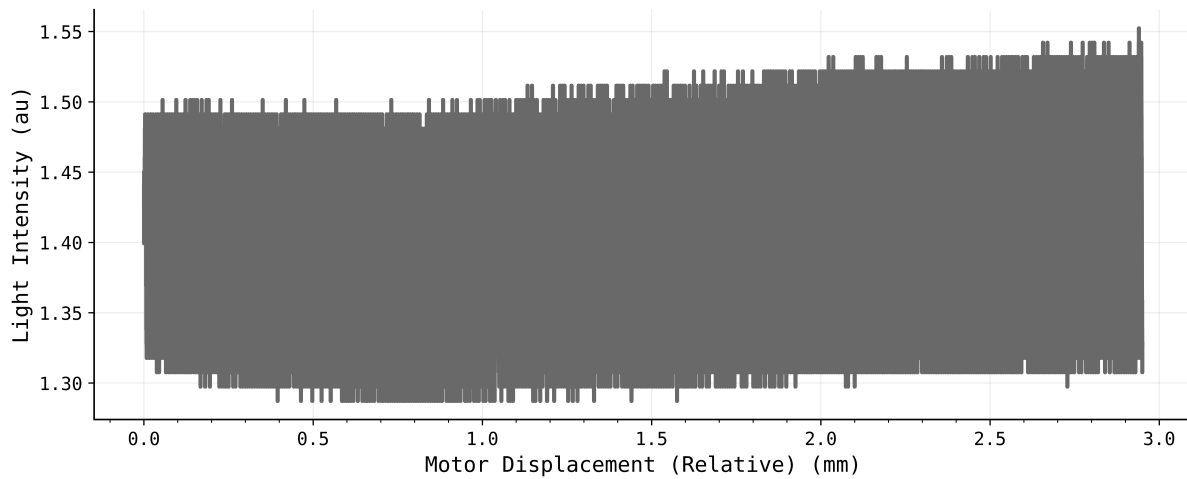
Appendix B

B.1 Calibration Raw Data



Move Relative Distance = 0.95mm | Data Displacement Step = 0.0002

Figure B.1: Intensity profile for relative motor displacement, corresponding spectrum shown in Fig 3.3.



Move Relative Distance = 2.95mm | Data Displacement Step = 0.0001

Figure B.2: Intensity profile for relative motor displacement, corresponding spectrum shown in Fig 3.4.

B.2 Unknown Diode utilised measurement

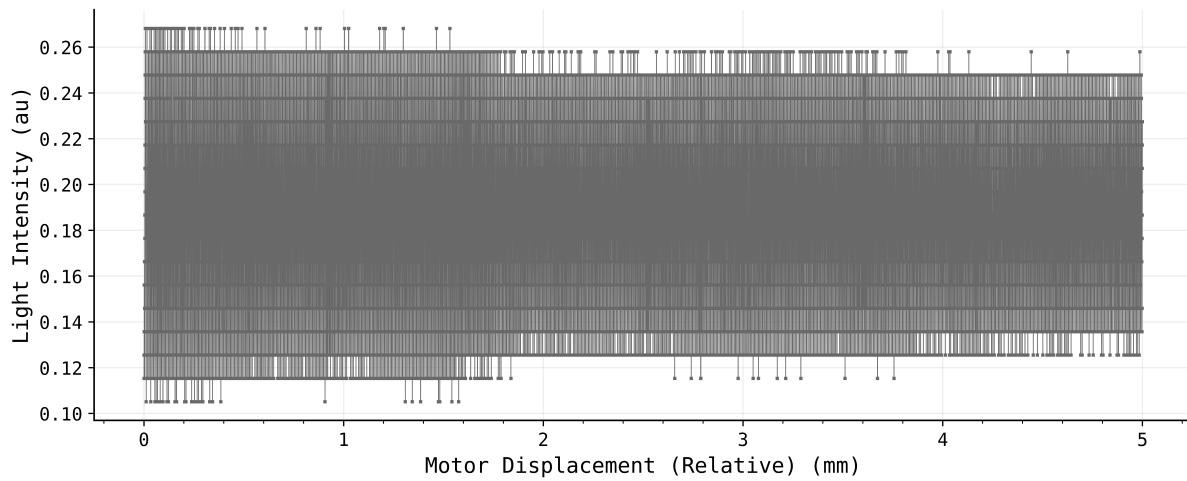


Figure B.3: Intensity profile for relative motor displacement, corresponding spectrum shown in Fig 3.5.

B.3 Refractive Index Measurement Relevant Data

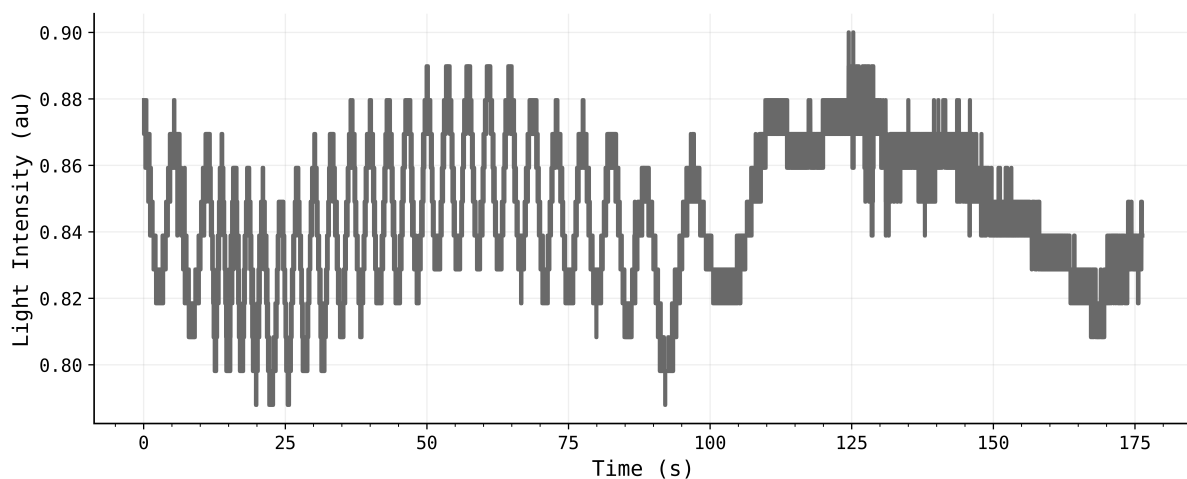


Figure B.4: Additional refractive index measurement #1. As the measurement began, air was reintroduced into the evacuated chamber by gently releasing the red valve at the bottom of the gauge. Data acquisition was stopped once the chamber was fully relieved. The number of fringes to be observed in this example is $m = 26$ not including the first.

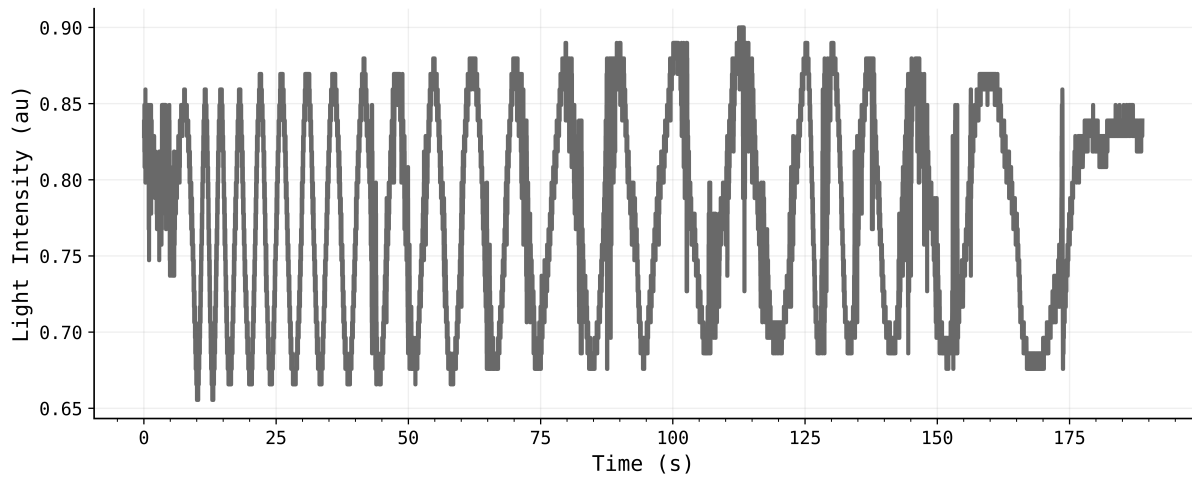


Figure B.5: Additional refractive index measurement #2. As the measurement began, air was reintroduced into the evacuated chamber by gently releasing the red valve at the bottom of the gauge. Data acquisition was stopped once the chamber was fully relieved. The number of fringes to be observed in this example is $m = 23$.

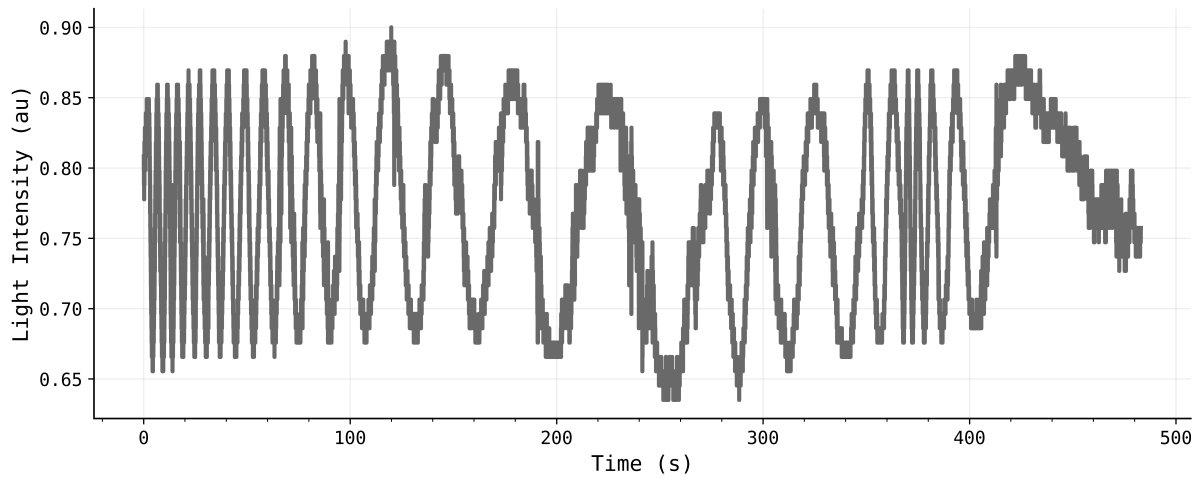


Figure B.6: Additional refractive index measurement #3. As the measurement began, air was reintroduced into the evacuated chamber by gently releasing the red valve at the bottom of the gauge. Data acquisition was stopped once the chamber was fully relieved. The number of fringes to be observed in this example is $m = 27$.

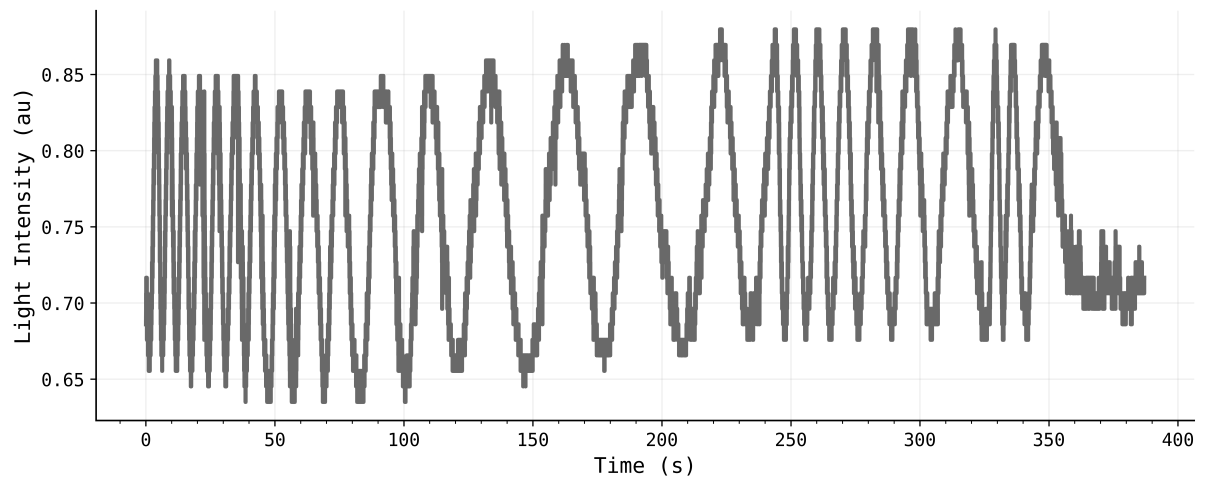
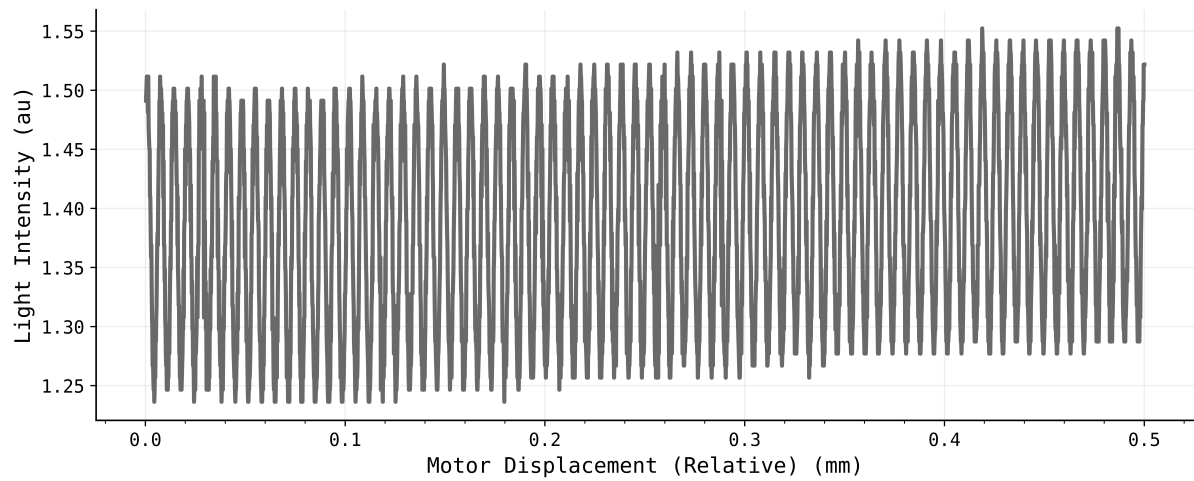
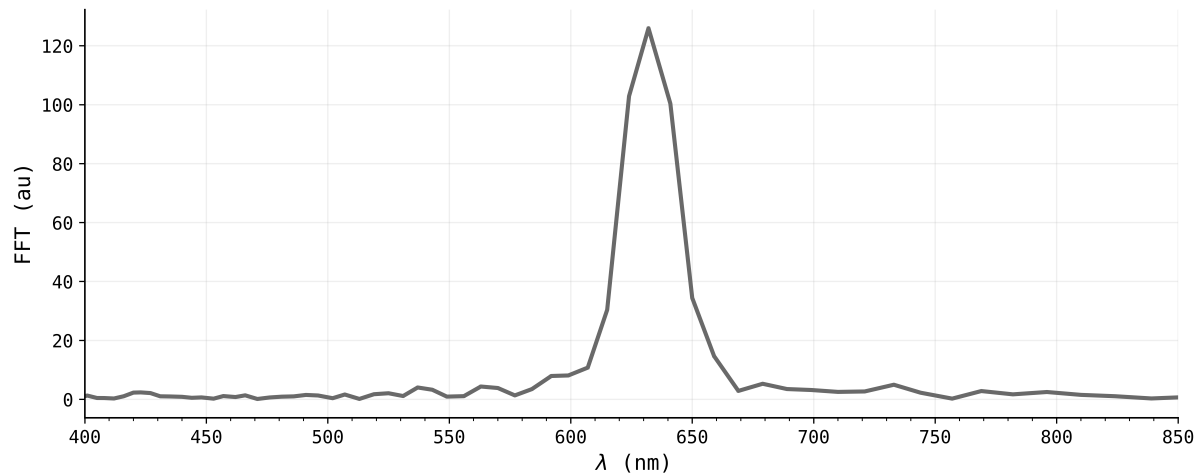


Figure B.7: Additional refractive index measurement #4. As the measurement began, air was reintroduced into the evacuated chamber by gently releasing the red valve at the bottom of the gauge. Data acquisition was stopped once the chamber was fully relieved. The number of fringes to be observed in this example is $m = 26$.

B.4 Other Measurements



(a) Raw Data



(b) Discrete Fourier Transform

Move Relative Distance = 0.5mm | Data Displacement Step = 0.0001

Figure B.8: Intensity profile for relative motor displacement and resulting transformation/frequency spectrum obtained from the procedure outlined in section 2.1.